Overdense Microwave Plasma Generation in a Negative-Permeability Space*)

Osamu SAKAI, Satoshi IIO and Yoshihiro NAKAMURA

Department of Electronic Science and Engineering, Kyoto University, Kyoto 615-8510, Japan

(Received 28 May 2013 / Accepted 11 September 2013)

High-power electromagnetic waves propagating in a negative-permeability space were investigated theoretically and experimentally, and they generated overdense plasmas successfully. Theoretical analysis predicted that high-density plasmas with negative permittivity can form via saddle-node bifurcations within an adequate electric field. To confirm theoretical predictions, using metamaterials with negative permeability achieved by magnetic resonances, we injected microwaves with several hundreds of watt into a waveguide filled with a low-pressure discharge gas. Langmuir probe measurement revealed that a generated plasma is well beyond the cutoff density for the wave frequency of 2.45 GHz, and indicated transition between positive-permittivity (low-electron-density) and negative-permittivity (overdense) states.

© *2013 The Japan Society of Plasma Science and Nuclear Fusion Research*

Keywords: microwave plasma, metamaterial, permeability, refractive index, bifurcation

DOI: 10.1585/pfr.8.1406167

1. Introduction

It is well known that electromagnetic waves propagate in a non-magnetized plasma with electron density n_e below the cutoff density [1]. We usually recognize such a feature using dispersion relation of electromagnetic waves [1], but we can also understand it from another point of view in which we use refractive index N, electric permittivity ϵ and magnetic permeability μ. ϵ in a plasma is expressed in the Drude model, and the waves can propagate in a region with $\epsilon > 0$, where $\epsilon = 0$ when the angular wave frequency ω is equal to the electron plasma frequency ω_{pe}. On the other hand, they cannot propagate in a region with $\epsilon < 0$ since N is imaginary when $\mu = 1$, which is the value of μ in conventional cases; note that $N = \sqrt{\epsilon}\sqrt{\mu}$ [2]. When we use plasmas generated by microwaves for industrial plasma processes, such prohibited propagation of the waves is an obstacle to achieve high throughput rates for material processing; at 2.45 GHz, which is the common frequency in commercially-available microwave sources, the waves cannot propagate in a high-n_e region beyond $7 \times 10^{10}\mathrm{cm}^{-3}$, which is insufficient n_e for usual plasma processes.

Along the above context, we can expect a completely different situation when μ is *negative*. In such a case, beyond the cutoff density, the waves can propagate because both ϵ and μ are negative and thus N is real and negative. In other words, high-n_e or overdense plasmas can be generated using microwaves by changing μ. A space with negative μ was realized using concepts and structures of metamaterials [3–5], in which a magnetic resonance makes macroscopic μ negative.

However, a few concerns remain before achievement of overdense plasmas, as shown in the following. When we consider evolution of n_e toward a state with negative N, we have to think about a transient state with $\epsilon > 0$ and $\mu < 0$, leading to imaginary N, in an initial phase of a low-n_e plasma. In such a case, the waves cannot propagate and remain evanescent. Furthermore, high-density microwave injection which induces n_e increments and evolution of n_e that affects ϵ are in a self-consistent relation, and a set of equations for this self-consistent analysis indicates that phenomena we have to clarify is in a nonlinear system. We investigated such a situation analytically in our previous report [6], but discussion performed there does not match specific experimental situations.

In this report, we theoretically analyze position-dependent balance between electric field and n_e in metamaterial structure with negative μ in a self-consistent manner, and derive bifurcation diagrams in this nonlinear system. This approach clarifies n_e and ϵ depending on initial microwave electric fields in bifurcation diagrams. Furthermore, we performed experiments of microwave plasma generation in a metamaterial with negative μ, and confirmed generation of an overdense plasma in single probe measurements in a bifurcated state.

2. Theoretical Analysis of Nonlinear System

To maintain complete self-consistency between energy of propagating microwaves and n_e in a generated plasma, numerical analysis including a fluid model [7] with particle balance and Maxwell equations [8, 9] is preferred,

author's e-mail: osakai@kuee.kyoto-u.ac.jp

*) This article is based on the invited talk at the 29th JSPF Annual Meeting (2012, Fukuoka)

© 2013 The Japan Society of Plasma Science and Nuclear Fusion Research

but it is rather difficult to extract underlying physics since calculated results obtained in numerical analysis are fairly complicated. Instead, we use here the method reported by our group recently [6], which is suitable for comprehension of physical processes and is reviewed briefly in the following.

The electric fields of both propagating and evanescent waves at spatial position $\boldsymbol{r}$ and time t have phase terms including N, given as

$$\boldsymbol{E}(\boldsymbol{r},t) = \boldsymbol{E}_0(\boldsymbol{r}) \exp\left(\boldsymbol{k}(\overline{N(\boldsymbol{r},t)}) \cdot \boldsymbol{r} - \omega t\right), \tag{1}$$

where $\boldsymbol{k}$ is wavenumber, $\omega/2\pi$ is frequency of the waves, and $\bar{x}$ means a spatially-averaged value of variable x. N is defined in regimes of metamaterials as

$$\overline{N(\boldsymbol{r},t)} = \sqrt{\epsilon(\boldsymbol{r},t)}\,\sqrt{\overline{\mu(\boldsymbol{r})}}. \tag{2}$$

μ is a macroscopic value determined by synthesized effects of array of metamaterial components, whereas ϵ is a microscopic value determined by collective effects of electrons in plasmas, given in the Drude model as

$$\epsilon(\boldsymbol{r},t) = 1 - \frac{\omega_{\mathrm{pe}}^2(\boldsymbol{r},t)}{\omega^2} = 1 - \frac{e^2 n_{\mathrm{e}}(\boldsymbol{r},t)}{\epsilon_0 m_{\mathrm{e}} \omega^2}, \tag{3}$$

where ω_{pe} is electron plasma frequency, ϵ_0 is vacuum permittivity, m_{e} is electron mass, and we assume collisionless plasmas. If plasmas are generated via electric-field drift motions of electrons and recombined with ions without spatial transport, the electron continuum equation based on particle balance is given as

$$\begin{aligned}\frac{\partial n_{\mathrm{e}}(\boldsymbol{r},t)}{\partial t} &= n_{\mathrm{e}}(\boldsymbol{r},t)\,\eta_{\mathrm{e}} E(\boldsymbol{r},t)\,\alpha(E(\boldsymbol{r},t),p) \\ &\quad -\beta n_{\mathrm{e}}{}^2(\boldsymbol{r},t),\end{aligned} \tag{4}$$

where η_{e} is electron mobility and β is recombination coefficient. The first term on the right hand side of Eq. (4) indicates production rate, and the second term represents recombination rate. Ionization coefficient α is

$$\alpha = Cp \exp\left(D\sqrt{\frac{E}{p}}\right). \tag{5}$$

Here, C = 29.2 and D = 26.6 for Ar gas [10] when we use α, p and E in the units of cm^{-1}, Torr and V/cm, respectively. In a steady state, n_{e} is as a function of E, derived from Eq. (4) as

$$n_{\mathrm{e}}(\boldsymbol{r},t) = \frac{1}{\beta}\eta_{\mathrm{e}} E(\boldsymbol{r},t)\,\alpha(E(\boldsymbol{r},t),p). \tag{6}$$

Equations (2)-(6) include E, ϵ and n_{e}, and we solve this nonlinear system by comparing two plots of E as a function of ϵ at each spatial position, which are derived from partial sets of equations as shown in the following. We used similar numerical results reported in Ref. [6] to derive E_{n}, which corresponds to E in Eqs. (1-3). Then, we set the parameter of Ar gas pressure to be 100 Pa, which was different from that in Ref. [6] and similar in the experiments shown in Sec. 3, and calculate E_{r} by Eq. (6). Finally, from points with $E_{\mathrm{n}} = E_{\mathrm{r}}$, we will obtain bifurcation diagrams which indicate ϵ transitions when we change injection power of microwaves P_{i} or electric field at the source point E_{i}. Note that n_{e} is uniform in the metamaterial region with slight spatial modulation that reflects discrete unit structures in the metamaterials working as boundary conditions for n_{e}, and loss mechanisms of electrons are recombination in a given position at which they are generated.

First, we explain the specific model used here and the results of theoretical analysis based on Eqs. (1-3) using Fig. 1. Figure 1 (a) shows the numerical model calculated by the finite-difference time-domain method. From the source, continuous sinusoidal waves at 2.45 GHz are launched, and the metamaterial region with $150\times200\,\mathrm{mm}^2$ has a value of $\mu = -1$. ϵ and μ in the surrounding region are both unity. By changing ϵ in the metamaterial region, we can derive stable values of the local electric field E_{n}. Note that near fields around the source point induce wave propagation inside the metamaterial region since the point source was so close to the region, by 10-mm distance.

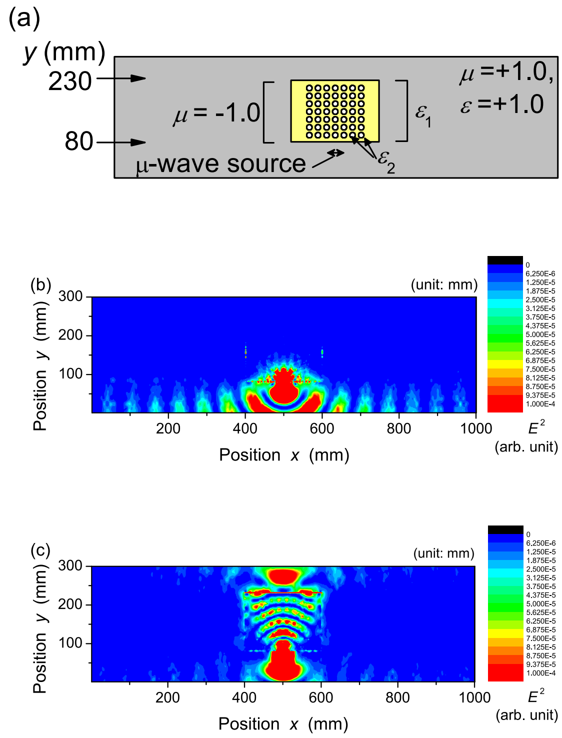

Fig. 1 (a) Two-dimensional configuration assumed in theoretical model. ϵ was slightly modulated to reflect differences of internal boundary conditions of metamaterial region with 150×200-mm area. Frequency of microwave is set to be 2.45 GHz, such as $|\epsilon_1 - 1|/|\epsilon_2 - 1| = 0.75$. (b) Electric field profile calculated in case with $\epsilon = 0.2$. (b) Electric field profile calculated in case with $\epsilon = -6.0$.

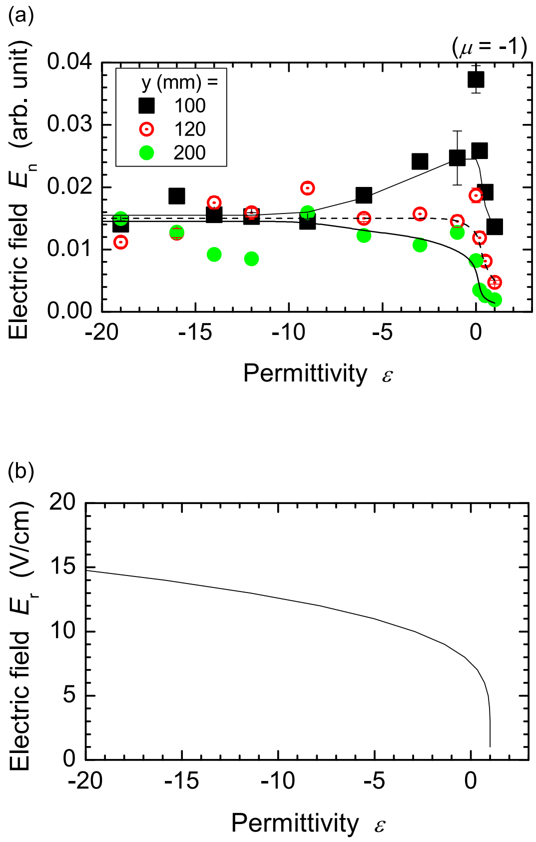

Fig. 2 (a) Electric field as a function of permittivity ϵ_1, calculated numerically in configuration shown in Fig. 1 (a). (b) Electric field as a function of permittivity ϵ_1, calculated theoretically from plasma particle balance.

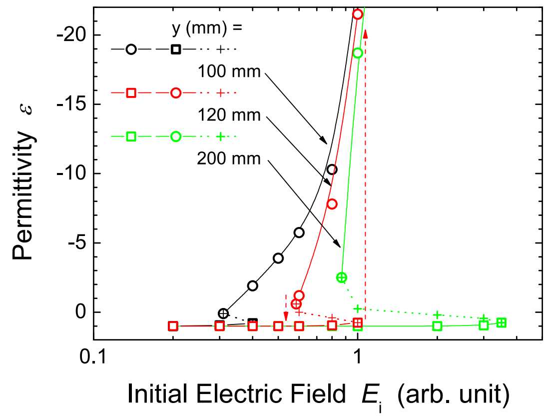

Fig. 3 Bifurcation diagrams of ϵ and initial electric field at microwave source, calculated using Fig. 2. Dashed arrows indicate partial phase portrait in case with y = 120 mm.

Figures 1 (b) and (c) demonstrate examples of numerical results. When n_e is low and ϵ is positive (Fig. 1 (b)), N is imaginary since μ is negative. As a result, the waves cannot propagate inside the metamaterial region. On the other hand, when the plasma is overdense and ϵ is negative (Fig. 1 (c)), they can propagate inside the region. These features are completely on the contrary to conventional cases with positive μ one of which is typically shown in Fig. 1 (b). When both ϵ and μ are negative, the phase velocity is reversed although the Poynting vector is forward from the wave source point [2].

After calculation of wave propagation in various cases of ϵ, we obtained local electric fields E_n at several points along the propagation path at x = 500 mm in Fig. 1. Figure 2 (a) shows the local electric fields calculated numerically. Due to the specific geometrical effects, we recognize irregular scattering of data, but roughly we can estimate dependence of the fields by solid curves as a function of ϵ. In all cases, the fields are almost the same when ϵ is fairly negative. On the other hand, at the points apart from the microwave source, we observe almost no electric fields when ϵ is positive. At the points that are very close to the microwave source, the fields are strong due to evanescent waves even in the cases with positive ϵ.

Electric fields are also calculated from Eq. (6), shown as E_r in Fig. 2 (b). We note that E_n is expressed in the arbitrary unit and linearly depends on E_i. That is, to see variation of n_e and ϵ as a function of E_i, the solutions are given by crossing points of E_r, which are the fixed values, and E_n with varying E_i.

Figure 3 shows ϵ dependences on the electric field at the source point of microwaves E_i, which is directly dependent on P_i. Note that solid and dotted lines indicate attractors with stable solutions and repellers with unstable solutions, respectively. At the position of y = 100 mm, evanescent waves with near fields are dominant, and we observe only a small bifurcation around $\epsilon \sim 0$ and hysteresis takes place with a small difference of E_i (0.3 - 0.4 in the arbitrary unit in Fig. 3).

At the position of y = 120 mm, propagating waves join evanescent waves which are depressed as the position becomes apart from the edge of the metamaterial region. As a result, clearer bifurcations are observed, and two saddle-node bifurcation points at $E_i \sim 1$ and 0.6 can be recognized. That is, as the working point goes up to $E_i \sim 1$, ϵ remains around +1. Then, at the bifurcation point around $E_i = 1$, ϵ jumps up to ~ -20, which indicates high-n_e plasma generation with $n_e \sim 10^{12}$ cm^{-3}. After the high-n_e plasma generation, as the working point goes down to $E_i \sim 0.6$, the plasmas are in overdense states with negative ϵ, and then, ϵ jumps down to $\sim +1$ around $E_i = 0.6$. In the case at y = 200 mm, around which the propagating waves are dominant, significant bifurcations with larger hysteresis are observed. In the cases at y = 120 mm and 200 mm, no plasma generation is expected at positive ϵ and the generated plasmas are always overdense.

3. Experimental Verification of Overdense Plasma Generation

To verify the above-mentioned theoretical predictions, we generated plasmas at low pressure using metamaterials

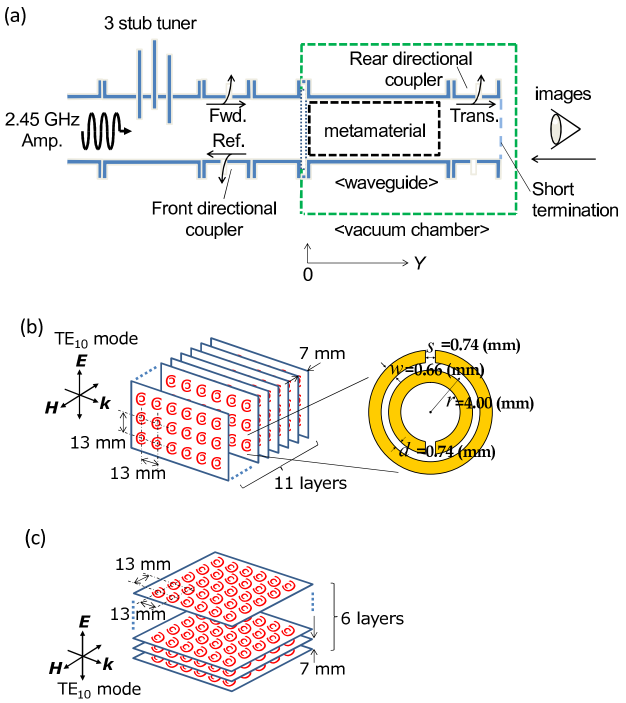

Fig. 4 (a) Experimental setup for plasma generation using negative-μ metamaterial. (b) Metamaterial structure leading to negative-μ state at 2.45 GHz. (c) Metamaterial structure leading to positive-μ state at 2.45 GHz.

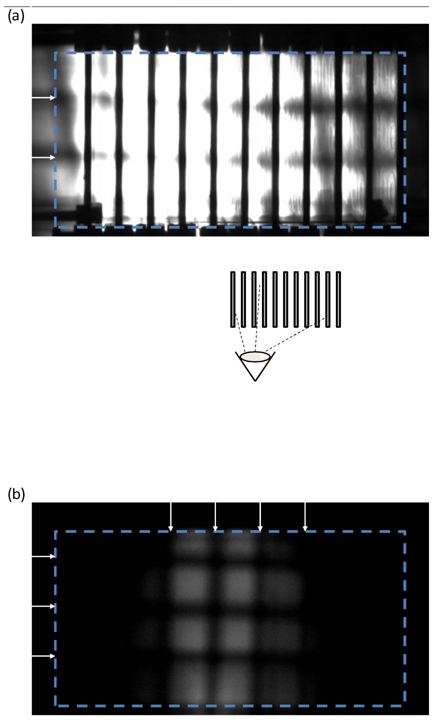

Fig. 5 (a) Visible image of plasma emission from metamaterial region shown in Fig. 4 (b). (b) Visible image of plasma emission from metamaterial region shown in Fig. 4 (c). In both images, dashed line indicates cross section of rectangular waveguide, and arrows indicate shadows of metal mesh which terminates microwaves at ends of waveguide.

with macroscopic negative μ. The experimental setup is shown in Fig. 4. The conventional rectangular waveguide at 2.45 GHz was installed in a vacuum chamber, which was filled with Ar at 100 Pa. This gas pressure assures generation of collisionless plasmas. We note that waveguide structure was almost kept both outside and inside the vacuum chamber, only with small discontinuity at the vacuum window made of teflon located at $Y = 0$ mm.

We set an array of double split ring resonators [3] as a negative-μ metamaterial for the region from $Y = 0$ to 80 mm; it consisted of designed copper films via a wet etching process from plane copper-covered glass-epoxy substrates. By derivation of the scattering parameters with the vector network analyzer (Anritsu Corp., MS2028B) and using the parameter retrieval method [11], we could estimate the value of macroscopic μ. In the case in Fig. 4 (b), the magnetic fields H penetrated the rings and we expected achievement of negative μ near their magnetic resonance, and μ was derived as −0.5 - 0.1 j at 2.45 GHz. On the other hand, in the case in Fig. 4 (c), the magnetic fields H never penetrated the rings and we could not expect negative μ since there were no magnetic resonances; as a result, μ was derived as ∼ +1 at 2.45 GHz.

Then, we injected 2.45-GHz microwaves with 360 W as a forward power with 25-µsec width from a high-power microwave amplifier (Kyoto-Micro-Densi, MA-02400C) into the vacuum chamber. Figure 5 (a) shows visible emission of plasmas generated in the metamaterial region of Fig. 4 (b). The images seemed to be inhomogeneous due to changes of the view angle, but they were uniform on the cross section of the metamaterial. From emissions near the right edge, we noticed that intensified emissions were near the entrance of the metamaterial region, and they decreases gradually as the microwaves propagated. In comparison, when we used another metamaterials structure, shown in Fig. 4 (c), whose DSRRs were perpendicular to those in Fig. 4 (b), we observed very weak and unstable emissions as shown in Fig. 5 (b). We note that we detected no signals above the detection limit of single Langmuir probes in the case shown in Fig. 4 (c); n_e was probably quite low below the cutoff density with $\epsilon > 0$ since $\mu > 0$.

Now we are concentrated on results of the negative μ metamaterial shown in Fig. 4 (b). Figure 6 (a) shows time evolutions of transmitted power detected by the directional coupler on the other side of the entrance. Without plasma generation, we did not detect any transmitted-power signals, unlike the forward- and the reflected-power signals. However, when the plasmas were generated, the transmitted power was detected, as shown in Fig. 6 (a), and *increased*. Such phenomena were not the case of microwave plasma generation in conventional schemes; usually, after plasma generation, the transmitted power decreases due to power dissipation. In our case, the change of N from the imaginary state with positive ϵ and negative μ to the real state with a double negative system induced enhancement

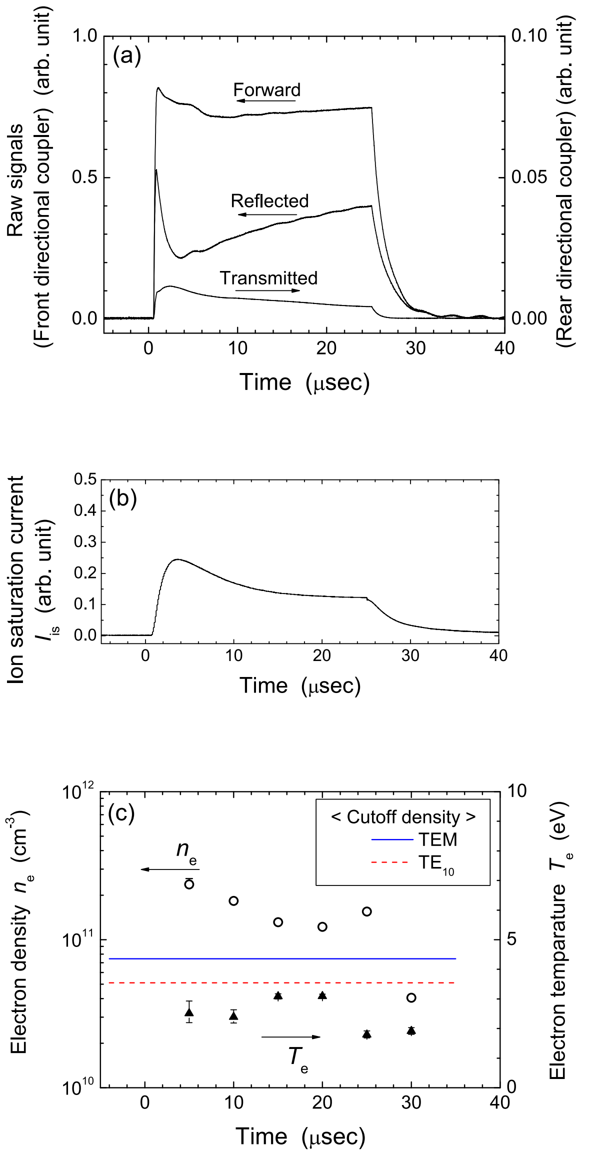

Fig. 6 Time evolutions of discharge signals in case of 2.45-GHz microwave injection at 360 W for forward power with metamaterial structure shown in Fig. 4 (b). (a) Forward, reflected and transmitted microwave power signals monitored at front and rear directional couplers. (b) Time evolution of ion saturation current measured at Y = 10 mm. (c) Time evolution of n_e (open circles) and T_e (closed triangles) measured at Y = 10 mm. Solid and dashed lines, expressed in left axis, indicate cutoff density for waves in TEM mode and for those in TE_{10} mode, respectively.

of transmittance. Figure 6 also shows ion saturation current I_{is} at −20 V measured by a conventional single probe at Y = 10 mm; this signal coincided with the power signals. By changing bias voltage, we obtained probe current-voltage curves in a few tens of shots. Figure 6 (c) shows evolution of n_e and electron temperature T_e. The solid line indicates the well-known cutoff density (7.4×10^{10} cm^{-3}) for waves in the TEM mode or propagating in an infinite plasma, and the dashed line indicates the cutoff density

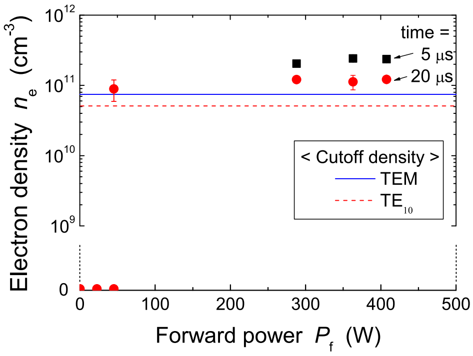

Fig. 7 n_e as a function of forward power measured at Y = 10 mm. Solid line indicates cutoff density for waves in TEM mode and dashed line indicates cutoff density for those in TE_{10} mode.

(5.1×10^{10} cm^{-3}) for those in the TE_{10} mode or propagating in an plasma occupying the rectangular waveguide. Monitored n_e is always well beyond the both cutoff densities when the microwave power was transmitted; overdense plasmas with negative ϵ were successfully generated.

Figure 7 shows variation of n_e as a function of the forward power P_f. When P_f was quite low (less than 40 W), we did not recognize any plasma generation, and when it was higher than 100 W, we always observed overdense plasmas. When P_f is around 50 W, we detected plasmas in some discharge shots and no plasmas in the other shots, and in the cases of plasma generation, we always observed overdense plasmas; we note that $\epsilon = 0$ at the cutoff condition, which is in the TE_{10} mode since we generated plasmas inside the waveguide. This experimental results indicate two possible states, with $\epsilon \sim +1$ and $\epsilon = -1$ - -2, similar to bifurcated solutions of n_e or ϵ for E_i = 0.6 – 1.0 at y = 120 mm shown in Fig. 3.

4. Concluding Remarks

We demonstrated overdense microwave plasma generation experimentally, which qualitatively coincides with the theoretical prediction. The theoretical analysis gave us bifurcation diagrams which indicated that overdense plasmas with negative ϵ and high n_e are generated in negative-μ space. The experimental results told us that overdense plasmas were certainly generated by microwave injection in a negative-μ space of metamaterials and that low density plasmas cannot be sustained in this metamaterial region. After high-n_e plasma generation, we observed enhancement of microwave transmittance. These facts indicate that overdense plasmas are generated in a negative-μ space, and that N becomes real and negative.

Acknowledgments

This work was partially supported by a Grant-in-Aid for Scientific Research from the Japanese Ministry of Education, Culture, Sports, Science and Technology.

[1] R.J. Goldston and P.H. Rutherford, *Introduction to Plasma Physics* (Institute of Physics Publishing, Bristol, 1995) p. 266.
[2] O. Sakai and K. Tachibana, Plasma Sources Sci. Technol. **21**, 013001 (2012).
[3] J.B. Pendry, A.J. Holden, D.J. Robbins and W.J. Stewart, IEEE Trans. Microw. Theory Technol. **47**, 2075 (1999).
[4] A. Sihvola (ed.), *Advances in Electromagnetics of Complex Media and Metamaterials* (Kluwer Academic, Dordrecht, 2002).
[5] L. Solymar and E. Shamonina, *Waves in Metamaterials* (Oxford University Press, Oxford, 2009).
[6] O. Sakai, J. Appl. Phys. **109**, 0849141 (2011).
[7] O. Sakai and K. Inoguchi, J. Phys. D **36**, 2491 (2003).
[8] Y. Takao and K. Ono, Phys. Plasmas **15**, 211 (2006).
[9] Z. Chen, S. Rauf and K. Collins, J. Appl. Phys. **108**, 073301 (2010).
[10] Y.P. Raizer, *Discharge Physics* (Springer, Berlin, 1987).
[11] D.R. Smith, S. Schultz, P. Markos and C.M. Soukoulis, Phys. Rev. B **65**, 195104 (2002).